

UDC 528.8.042.1

GOOGLE EARTH ENGINE FOR LANDSAT IMAGE PROCESSING AND ASSESSING LULC CLASSIFICATION IN SOUTHWESTERN CÔTE D'IVOIRE

Christian Jonathan Anoma KOUASSI¹, Chen QIAN¹, Dilawar KHAN¹, Lutumba Suika ACHILLE¹, Zhang KEBIN¹, James Kehinde OMIFOLAJI^{2,3}, Xiaohui YANG^{4*}

¹*School of Soil and Water Conservation, Beijing Forestry University, Beijing, China*

²*School of Ecology and Nature Conservation, Beijing Forestry University, Beijing, China*

³*Department of Forestry and Wildlife Management, Federal University Dutse, Jigawa State, Nigeria*

⁴*Institute of Desertification Studies, Chinese Academy of Forestry, P. O. Box 35, Yiheyuanhou, Haidian District, 100091 Beijing, China*

Received 07 April 2022; accepted 17 February 2023

Abstract. High-accuracy land use and land cover maps (LULC) are increasingly in demand for environmental management and decision-making. Despite the limitation, Machine learning classifiers (MLC) fill the gap in any complex issue related to LULC data accuracy. Visualizing land-cover information is critical in mitigating Côte d'Ivoire's deforestation and land use planning using the Google Earth Engine (GEE) software. This paper estimates the probability of RF classification in South Western Côte d'Ivoire. Landsat 8 Surface Reflectance Tiers 1 (L8OLI/TIRS) data with a resolution of 30 m for 2020 were used to classify the western and southwestern Forest areas of Côte d'Ivoire. The Random Forest (RF) learning classifier was calibrated using 80% training data and 20% testing data to assess GEE classification accuracy performance. The findings indicate that the Forest land class accounts for 39.48% of the entire study area, followed by the Bareland class, the Cultivated land class 21.28±0.90%, the Water class 1.94±0.27%, and the 0.96±0.60% Urban class respectively. The classification reliability test results show that 99.85%±1.95 is the overall training accuracy (OTA), and 99.81±1.95% for the training kappa (TK). The overall validation accuracy (VOA) is 94.02±1.90%, while 92.25±1.88% validation kappa (VK) and 92.45±1.88% RF Accuracy. The different coefficients classification accuracy results obtained from the RF confusion matrix indicate that each class has three good performances. This is due to the cultivated land samples lower spatial resolution and smaller sample numbers, resulting in a lower PA for this class than for the other classes. All had producer accuracy (PA) and user accuracy (UA) more than 90% using the L8OLI/TIRS data. Using the RF-based classification method integrated into the GEE provides an efficient and high scores accuracy for classifying land use and land cover in the study area.

Keywords: supervised classification, land-use/land-cover, Google Earth Engine, Random Forest, accuracy assessment, deforestation.

Introduction

LULC is essential in regional planning, environmental research, and understanding the environment (Foody 2002; Parente & Ferreira, 2018). Land-use types have been found to have a substantial effect on runoff reactions in catchments (Cecchi et al., 2009). This impact is amplified much more in highly anthropogenic areas (crops, rangelands, etc.).

Furthermore, land use affects biogeochemical cycling, global warming, land erosion, and sustainable development. Landscape changes have an increasing influence on climate change, atmospheric nitrogen deposition, and

biological invasions, in addition to their effect on biodiversity (Thébault & Loreau, 2005). Because of the extensive availability of satellite data in recent years, one of the most sophisticated fields of environmental remote sensing is identifying abrupt changes in forest ecosystems. Over the past several decades, the improved availability of remote sensing data in terms of spectral and high temporal, together with lower acquisition and processing costs, has resulted in greater use of these data's enormous potential for studying the Earth's surface (Cohen et al., 2010; Kennedy et al., 2010; Tassi et al., 2021). Recent advancements in satellite data processing have been enabled by cloud-based systems that provide users with free access to

*Corresponding author. E-mail: yangxh@caf.ac.cn

extensive geospatial data and faster analysis through web-site interfaces. Google Earth Engine (GEE) is now one of the most commonly utilized systems, providing remote sensing data's main storage, compilation, processing, and analysis needs (Gorelick et al., 2017).

This platform includes a variety of methods for LULC classification based on robust algorithms. Its consumer interface and straightforward JavaScript language allow the developed script to be readily reproduced and exploited through the cloud platform.

Therefore, land-use analysis information is always helpful in creating appropriate strategies for better managing the land-use situation. Many methods have been devised and utilized to accomplish this objective, with varying degrees of success (Mas, 2000; Lu et al., 2006).

Indeed, the implementation of RF in GEE has shown its capacity to provide outstanding results in various applications, including the processing of substantial long-term global-scale datasets (Magidi et al., 2021). GEE has a reputation for analyzing the impact of land-use change on urban surface heat by leveraging an already established climate tool to extract massive land surface temperature data (Robinson et al., 2017; Ravanelli et al., 2018) and predicting vegetation phenology (Parente & Ferreira, 2018; Traganos et al., 2018). Many authors have employed this platform with RF in numerous areas of research, including forest change detection (Moore & Hansen, 2011; Hansen et al., 2013), habitat monitoring (Joshi et al., 2016), urban area mapping (Liu et al., 2018), and human activity detection (Benz et al., 2017).

Land-cover change has been identified as the most critical anthropogenic disturbance of regional character regarding environmental implications for people (Walker, 2004). Essentially, LULC changes result from dominant natural and anthropogenic processes interacting via human activities. As a consequence, changes in land use and cover, as well as deterioration, are all governed by the same fundamental reasons.

Therefore, changes in land-use and land-cover and impact biogeochemical cycling and subsidence pathways (Verburg et al., 2006) and a wide range of socioeconomic and ecological processes (Desanker et al., 1997) are critical to understanding managing environmental mechanisms and management. Significant advances in remote sensing methods for LULC research have allowed the development of a massive dataset of collected and processed satellite images and a large number of machine learning algorithms for supervised image classification across a wide range of domains (Caruana & Niculescu-Mizil, 2006).

As a result, it is widely accepted that among the various measures available, overall accuracy (OA) is used to assess the performance of all classifiers as well as the effect of sampling designs through the implementation of one of the classifiers, namely RF, is used to assess the performance of all classifiers in the production and exploitation of results (Mellor & Boukir, 2017). OA is the most often used measure since it is easy to comprehend and estimate in various scenarios (Plourde & Congalton,

2003). It denotes the classifier's rate of test data correctly classified using the classification method. As an additional benefit, OA is an indicator of classifier performance that may be used to assess a specific classifier's performance at the class level (Gorelick et al., 2017).

The collecting and processing of primary data with RF in GEE enable the user to quickly develop a multi-temporal filtered data set, which is essential for computing a more accurate classification of LULCs (Griffiths et al., 2013). For example, at an atmospheric surface reflectance (SR) processing level, 30 m L8 bands are now accessible in GEE (Gorelick et al., 2017). Many studies have employed the RF method in GEE to enhance the pixel-based classification of LULC (Xiong et al., 2017; Mahdianpari et al., 2019; Ghorbanian et al., 2020). RF is the most widely used machine learning method in the GEE application and, in general, for the classification of satellite data because of its non-parametric nature, ability to handle dimensionality and overfitting, and overall superior performance compared to other classifiers (Mountrakis et al., 2011; Rodriguez-Galiano et al., 2012a, 2012b; Belgiu & Drăguț, 2016; Nery et al., 2016; Amani et al., 2020; Naboureh et al., 2020). The RF is built on numerous Classification And Regression Trees (CART), with the prediction model based on the average of all these CARTs (Athey et al., 2019). RF has been employed successfully in GEE in several LULC studies (Corona et al., 2012; Rodriguez-Galiano et al., 2012a; Adelabu et al., 2015; Meher et al., 2016; Probst & Boulesteix, 2017; Phan et al., 2020; Luo et al., 2021; Magidi et al., 2021; Tassi et al., 2021).

RF classification techniques for surface reflectance images based on cloud, shadow, and pixel removal utilizing Function of Mask (FMASK) and metric-based composites in GEE, for example, have been evaluated with an overall accuracy of more than 85% to identify farmland from non-cropland (Azzari & Lobell, 2017).

RF improves LULC mapping accuracy compared to other prominent comparable methods (Zeferino et al., 2020). When the class size distribution is imbalanced, it preserves the classification error balancing (Hatwell et al., 2020; Magidi et al., 2021). Because it derives the data characteristics autonomously, the RF classifier needs little or no user involvement, simplifying its design process (Toosi et al., 2019). Even though the RF method offers various data characterizations, it has a relatively fast processing speed (Schmidt et al., 2019; Gudmann et al., 2020). Barlett et al. (1998) demonstrated that RF may substitute the missing values with a variable that often occurs in a particular node in data loss. Because of its capacity to increase mapping accuracy, RF has been applied in various research fields (Magidi et al., 2021).

Additionally, GEE provides methods to evaluate the accuracy of different classifiers, such as error matrices (Stehman, 2009). Previous land-use and land-cover mapping investigations in the southwest area of the Côte d'Ivoire related significant human pressures due to the conversion of large expanses of the forest into agricultural land (Barima et al., 2016, 2020; Kouassi et al., 2021). This

region is dominated by export crop production, accounting for over half of total cocoa output in the nation (Ruf & Zadi 1998; Koua et al., 2020). Each year, hundreds of hectares of forests are taken from national parks and protected areas, a process known as deforestation (Ruf et al., 2015; Koua et al., 2020). This is an important finding since it suggests that forest destruction is rising at a nearly exponential pace.

Given this situation and the expansion of unplanned urban infrastructure zones, industrial and artisanal mining, and its environmental effect, it is critical to conduct an inventory of this critical zone, which contains more than two-thirds of Upper Guinea’s endemic forests (Chatelain-Ponroy, 2010; Bitty et al., 2015). Numerous applications depend on precise and up-to-date land cover change information, which is challenging to get specialized expertise. In light of environmental issues and problems, there is a significant need for information on the accuracy of

maps as a result. Many people now consider the evaluation of the precision of maps to be a critical component of many cartographic projects of maps to be a vital component of any cartographic project they are involved in (Cihlar, 2000; Strahler et al., 2006).

The study aims to assess and classify the land-use land-cover of the country’s southern-western region using the GEE Application Programming Interface (API) to map land-cover using the RF approach based on high spatial and temporal resolution pixels the southwestern part of Côte d’Ivoire.

1. Methods

1.1. Study area

Côte d’Ivoire is a West African nation on the Atlantic Ocean (Figure 1). It covers 322 462 km² of land. The flora of Côte d’Ivoire is divided into four types: dense tropical

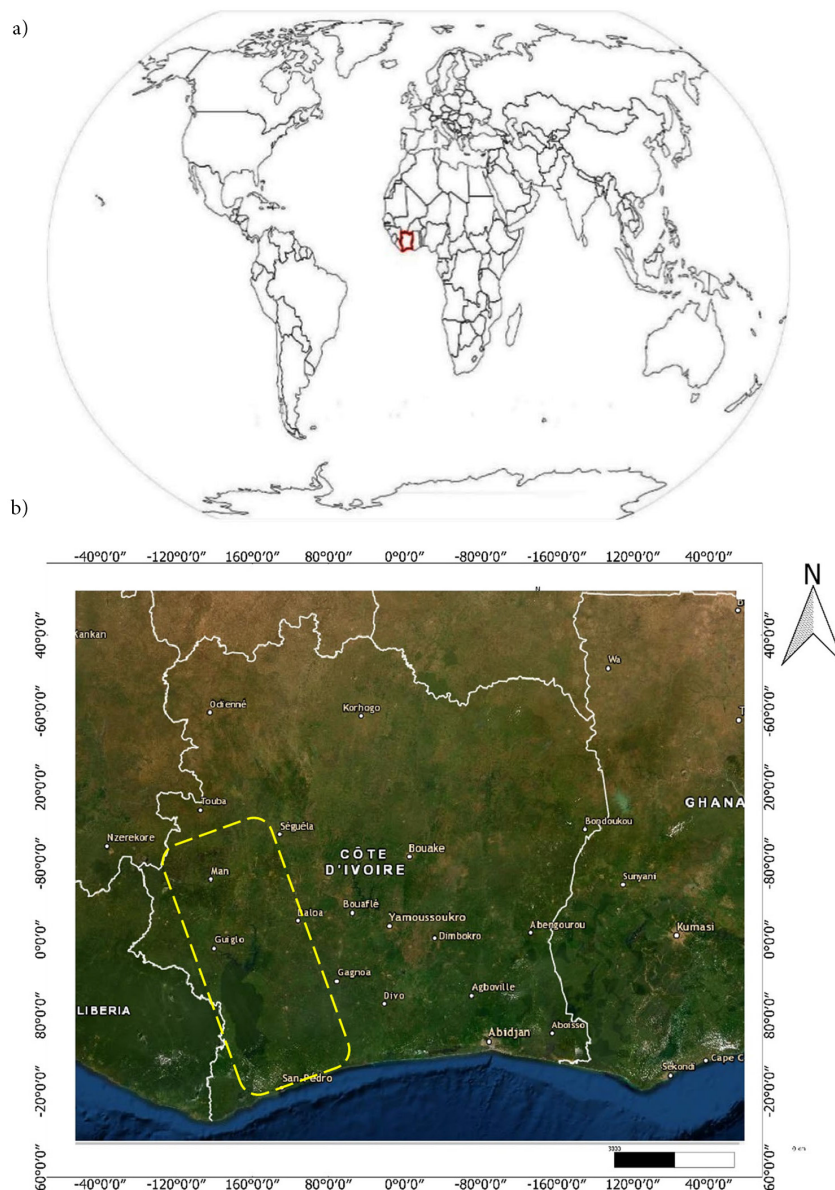


Figure 1. Map of the study area: a – World map with Côte d’Ivoire; b – Côte d’Ivoire map with study area

forest, semi-deciduous forest, evergreen rainforest, and wooded to grassland savannah. The southwest of Côte d'Ivoire is notable for its unique species and biodiversity. The country's first ecological zone lies in the south. There was a dense, humid forest covering this area, but it was severely destroyed. Côte d'Ivoire has a sub-equatorial climate with four seasons and 1200–1500 mm annual rainfall. A dense west forest covers the southern part of the middle half of the Guinean-Congolese/Sudanese region transition (White, 1983). The study area has a network of forest classifications and national parks, the most notable being Tai National Park (TNP). The TNP is the remnant of $\frac{3}{4}$ of the hyper ombrophilic forest of Côte d'Ivoire. This represents about 25% of the Ivorian rainforest. TNP also constitutes more than half of the mammal species of the West African forest zone. This exceptional richness has justified the classification of TNP by UNESCO as a biosphere reserve and world heritage site (Chatelain et al., 2004).

1.2. Data processing in GEE

The classification and accuracy validation methods were implemented in a single GEE script and verified based on the classification and accuracy evaluation processes. The former comprises a Pixel-Based technique, utilizing the same training data and the RF algorithm to get their results. The confusion matrix is generated by applying the RF classifier to the same training and validation data. These methods are based on pixels, objects, or a combination of the two, and they use either a supervised classification technique like RF (Gislason et al., 2006; Tatsumi et al., 2015; Wang et al., 2015) that we use (Figure 2).

1.3. Random Forest Method

The RF approach is a very well non-parametric machine learning technique. RF was selected for this study because it produced almost as accurate quality results for land use classification even when no hyperparameters were used. It is appropriate for both classification and regression tasks. Furthermore, the RF classifier provides higher classification accuracy (Qu et al., 2021). Its use in remote sensing has various benefits, including improved accuracy of land use and land cover mapping compared to other prominent algorithms (Zeferino et al., 2020). The RF technique stabilizes the classification error balance when skewed class size distribution (Toosi et al., 2019).

The RF classifier eliminates data characteristics. When utilized in its operational mode, the RF method has a quick execution time in terms of processing time (Forghani-Zadeh & Rincón-Mora, 2007). GEE's RF execution method is pixel-based because it is resistant to data noise and overfitting (Belgiu & Csillik, 2018). Its low sensitivity to overfitting is helpful for satellite data categorization (Keyport et al., 2018). RF is an ensemble learning approach that employs many individual decision trees (Fonseka et al., 2019). Each decision tree has numerous nodes, and a majority vote determines the ultimate conclusion among those who participated. The benefit of utilizing this classifier is that it may offer a highly accurate classifier capable of handling hundreds of input variables (Ge et al., 2019).

According to Breinam (2001) RF has many classifiers defined by the following (Equation (1)) (Breiman, 2001).

$$\{DT(y, \sigma i_{i=1}^T)\}, \quad (1)$$

where y is the input vector and σi is a random vector sampled independently but with the same distribution as the preceding $\sigma i, \dots, \sigma i - 1$. T bootstrap provides from training data. Each bootstrap sample yields a no-pruned classification, and a regression tree is drawn for each bootstrap sample β with just one of M randomly selected characteristics chosen for the split at each point of the CART.

The RF is more robust to minor changes in input data and improves LULC classification performance by stabilizing the classifier. Bootstrap selection retrieves i samples from the training sample set, each equal size. For each sample, i trees were created, producing i classification results. The final LULC classification was determined by classifying accuracy utilizing each record. The RF classifier enhances classification accuracy using object-based processing approaches (Gislason et al., 2006).

1.4. Accuracy Assessment

The confusion matrix (CM) is crucial in the map classification validation process.

It compares the anticipated class label to the ground reference. Accuracy measures such as overall accuracy, Kappa, and user precision may be calculated using the confusion matrix (Foody, 2002). The Kappa, user accuracy, and producer accuracy score are calculated for each class. The proportion of pixels with the correct label is referred to as overall precision. It is frequently referred

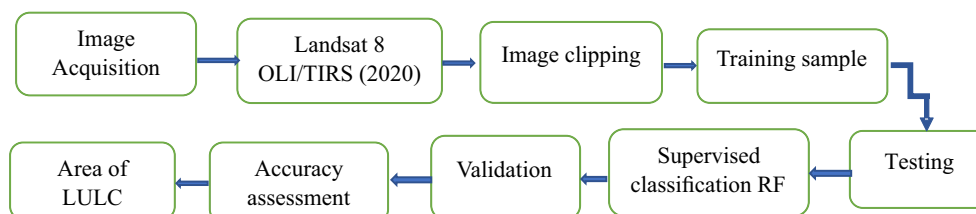


Figure 2. The flow chart of the methodology implemented in GEE

to as an indicator of general agreement between the classification and the ground reference (Foody, 2002). If the operator wants to concentrate on a specific precision class, both the user and the manufacturer must be precise. “User accuracy” refers to the proportion of erroneously categorized pixels into a recognized category.

A CM included in GEE is used to determine the accuracy of the study area LULC categorization. The LULC linked with the validation point is statistically compared with the output classifications. To evaluate the classification’s performance, the kappa coefficient and the values of the confusion matrix’s overall user, producer, and accuracy coefficients were compared for each class (Forghani-Zadeh & Rincón-Mora, 2007). The image classification accuracy was assessed using RF’s confusion matrix (Congalton & Green, 2019).

1.5. Training and validation sample data

We used cloud computing for the pixel-based RF machine learning technique implemented in GEE cloud computing to categorize the study area based on pixels to classify LULC. This research’s training and validation samples were gathered via manual visual interpretation of high-definition images from Google Earth. We selected training and validation point. Finally, we were awarded 874 points for training and validation. We utilized 80% of the pieces for training and 20% of the testing to assess accuracy. The algorithm used 690 points for training and 184 for testing. The RF model was constructed using 300 trees and five predictors chosen at random from a vast pool of candidates (such as “B3”, “B4”, “B5”, “B6”, and “B7”). Table 1 shows the number of training points in the study area for the selected classes.

Table 1. Number of validation for each land-use and land-cover class

Classes	Validation training point
Forest	261
Water	181
Urban	214
Cultivated	79
Bare land	139

1.6. Data

For this study, we used the Landsat-8 Operational Land Imager (OLI)/Thermal Infrared Sensor (TIRS) surface reflectance (SR) 30 m T1 dataset immediately accessible year is 2020. We utilized the method provided in the literature to evaluate the overall dependability of the process, as suggested by (Hansen et al., 2008) and (Bwangoy et al., 2010). To gather training data, only 50 points from each class were identified utilizing the GEE interface, the composite Red-Green-Blue (RGB) and infrared layers, and the high-resolution layer of Google Maps. A total of 874 validation points were generated at random and manually

labeled using visual interpretation of the experiment’s identical base layers. Rodriguez-Galiano et al. (Rodriguez-Galiano et al., 2012b) and Pareeth et al. (Pareeth et al., 2019) show that the main band components may increase LULC classification accuracy. As a result, the red, green, blue, near-infrared (NIR), and shortwave infrared (SWIR-1 and SWIR-2) bands were considered in this Landsat-8 OLI image analysis.

1.7. Landsat data

Operational Land Imager (OLI) mission, the most recent phase of this paper, relied heavily on Landsat 8 surface reflectance (SR)/OLI 30 m satellite data. Indeed, the Landsat-8 (L8) Operational Land Imager (OLI) mission, the most recent phase of the National Aeronautics and Space Administration (NASA) Landsat Data Continuity Mission (LCDM), is effective of delivering datasets that are spectrally, spatially, and temporally compatible with primary Landsat missions (Irons et al., 2012). Landsat is the only medium-resolution land-use dataset that can be used to investigate changes in LULC throughout any period and terrain type, according to LCDM (Pareeth et al., 2019)). L8SR/OLI sensor characteristic has to revisit 16 times. It can provide multispectral images with 30 m resolution, including its five visible and near-infrared (VNIR) bands, two infrared and two shortwave infrared (SWIR) bands.

1.8. Processing

We first uploaded the L8SR images into GEE and then used the L8 SR data to build a cloud mask function from the pixel quality attributes “Pixel_QA” band C Function of Mask (CFMaskAlgorithm). Cloud may be removed from the L8SR using the “Pixel-QA” band, a bitmask band containing a quality indicator generated using the CFMASK technique (Foga et al., 2017). The cloud shadow is indicated by bits 3 and 5 when viewing the L8SR image. We performed data filtering using the “CloudshadowBitMask” technique for bands B3: (Cloud Shadow) and B5: (Cloud Shadow). We created a Mask function on the L8SR image collection to display the pixel’s precise conditions on the mask image. We applied it to the L8SR image collection, using the B3: (CloudShadow Pixel 3) and B5: (pixel), each pixel equal = 0. To be utilized with the clouds, a new variable “bitwise and” was created and put on the bands B3: “CloudShadowBitMask” and B5: “CloudMask”. We designed a “updateMask” function by dividing the bands from 0 to 9 by ten thousand. After modifying a year list to filter out the bands from the photo collection, we masked out the clouds and reduced the size of the images.

GEE achieved cloud masking for L8SR by combining the Pixel Quality Attribute (PQA) band with the L8SR data after image processing and before any pre-processing (Lu et al., 2006).

According to Nyland et al. (2018), the cloud masking step should be carried out in line with their recommendations, which include, among other things, picking the

input photographs with the highest degree of cloud cover and three perimeters to construct an exceptionally efficient composite image.

Foga et al. (2017), suggest that GEE classification be conducted using supervised classification, which considers the collection of training points and the kind of classification performed in general while making the classification (Foga et al., 2017). Consequently, to assess whether or not the model is accurate, the validation points were generated at random and manually labeled with the same LULC code.

The land cover categorization of the study area was achieved using a pixel-based supervised classification approach combined with an RF machine learning algorithm. Following an assessment of the composite images, it was concluded that the Google Earth images should generate training and test polygons as a starting point. Five land classifications were defined based on land use information acquired for the study area: Forest, Water, Urban, Cultivated, and Bareland. The land classes identified were forest, water, urban, cultivated, and bare land (Table 2). The acquired samples were then used for RF training with the assistance of GEE.

For the use of RF models in GEE, two parameters were defined: the number of decision trees (“(300,5)”) to be produced per class (number of trees) and the random selection of 5 predictors per class (number of trees). A last morphological operation (based on a focused mode) is performed on the output classification to clean up the whole output and decrease the “salt and pepper” impact. The training was carried out using bands and the land cover property, followed by the extraction of the land cover property of the various classes. This classifier was developed using training data from the feature collection new feature collection (Newfc) attribute “LULC,” which was collected from the feature collection “Newfc.” Consequently, the bands [“B3”, “B4”, “B5”, “B6”, and “B7”] were used as prediction bands for the LULC classification, and the LULC classification was formed from them.

Table 2. Land-use/land-cover classification

Land classification	Description
Forest	*Forest, natural or planted forests, Deciduous forest land, evergreen forest land, mixed forest land
Water	*Lakes, rivers, marries, wetlands, reservoirs, streams and canals, reservoirs, bays, and estuaries
Urban	*Built-up area of all settlements, including industrial zones and other artificial surfaces
Cultivated	*Cropland and pasture, perennial and annual crops, including various crops such as cereals, grain legumes, and horticultural plants, another agricultural land
Bareland	*Bareland, exposed rock, strip mines, quarries, gravel pits, transitional areas, mixed barren land

Some samples were randomly separated and utilized in testing to assess the model’s accuracy, while others were used in training. Approximately 80% of the samples were used in training, whereas 20% were used in testing.

We evaluated whether the classification model was accurate based on the matrix confusion formed by RF integrated into the GEE. The LULCs linked with the validation points are statistically compared to the output classifications.

2. Results

To categorize the study area using LULC, a modified version of GEE’s integrated automatic classification system was used. The error-based accuracy assessment assesses the image’s quality generated using the RF model. The processing results show that the Training Overall Accuracy (TOA) is 99.85%±1.85, and the TK is 99.81±1.95, in that order. Similarly, the OVA RF model received 94.02%±1.90 against VK and 92.25%±1.88 against VK (Figure 3).

The finding revealed confusion between Forest, Water, Urban, Cultivated, and Bare land classifications. It is followed by forest land, which covers 22870.53 km², or about 39.62%±1.23. Forest land is more dispersed in the upper central region of the map, dominated by TNP, which covers a relatively significant area in terms of forest class, and farther north of the study area, scattered regions that host national reserves with neighboring states. The water-covered zone, which amounts to 951.97 km² (1.64%±0.25 of the study area), is near the TNP and south of the study area. The urbanized aera comprises numerous developed regions scattered throughout the study area. In the southern hemisphere, Urban accounted for about 555.06 km² or 0.96%±0.60 of the total land area.

The Cultivated class will cover about 12284.66 km² or 21.28%±0.90 of the study area. It covers about 21056 km² or 36.48%±1.18 of the total Bareland area. The confusion matrix is the beginning point for examining the assessment data (Story & Congalton, 1986). The GEE method produces separate sets of confusion and accuracy matrices depending on the number of included and non-included pixels in the splits samples, in line with the random training and testing procedures used for sample splitting (Table 3). The confidence level was used for calculating the confidence intervals (95%). The 95% confidence intervals for all accuracy metrics were determined by multiplying

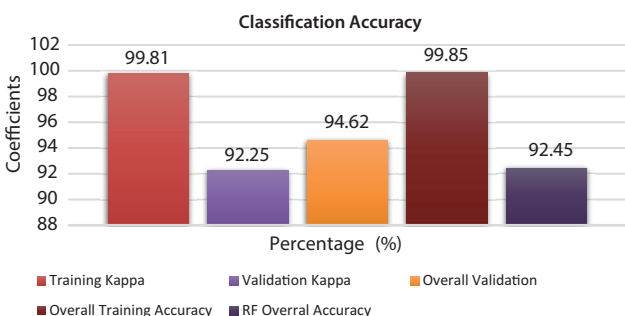


Figure 3. Percentage of different coefficient obtained by RF

Table 3. Global confusion matrix of RF classification results

Class	Forest	Water	Urban	Cultivated	Bare land	Total	PA (%)
Forest	205	0	0	3	0	208	98.55±1.96
Water	0	151	0	0	0	151	100±1.96
Urban	0	0	175	0	9	184	95.1±1.91
Cultivated	11	0	6	60	4	81	74.07±1.68
Bare land	4	0	8	2	111	125	88.8±1.88
Total	220	151	189	65	124	749	–
UA (%)	93.18±1.89	100±1.96	92.59±1.88	92.3±1.88	88.7±1.84	–	–

the square root of the variance by 1.96 (Olofsson et al., 2014). Furthermore, the training and test set selection affected the validation and classification accuracy for random splitting.

For the RF performance calculations in GEE, the coefficients of user accuracy \hat{U} (Equation (3)), (Story & Congalton, 1986) as well as producer accuracy \hat{P}_j (Equation (4)) (Congalton & Green, 2019), were used to assess classification accuracy. In addition to the calculations of \hat{U}_i and \hat{P}_j we calculated estimates of the accuracy of our final change map by combining Equations (3) and (4).

User accuracy \hat{U}

User’s accuracy is the proportion of the area class i that is also class i in the reference data (Equation (3)). It provides users with the probability that a particular class i is also that class on the ground.

$$\hat{U}_i = \frac{\hat{P}_{ii}}{\hat{P}_i} \times 100, \tag{3}$$

\hat{P}_j is the estimated proportion of area in cell, j of the error matrix. i and j are the rows and columns of the confusion matrix (Table 3).

\hat{P}_{ii} is the estimated proportion of area in cell, i of the error matrix. i and i are the rows and columns of the confusion matrix.

In the reference data, 205 of the 208 pixels categorized as Forest were recognized as Forest; 3 Cultivated were included in the Forest categorization.

Of the 151 pixels, all were identified as Water.

In the reference data, 175 of the 184 pixels classed as Urban was recognized as urban; 9 Bareland areas were included in the Urban categorization.

In the reference data, 60 of the 81 pixels classed as Cultivated were recognized as Cultivated, with 11 Forest, 6 Urban, and 4 Bareland included in the Cultivated.

Of the 125 pixels classed as Bare land, 111 were recognized in the reference data as Bare land, 11 Forest, 6 Urban, and 4 Bare land were included in the Cultivated data.

Producer’s accuracy \hat{P}_j

Producer’s accuracy is the proportion of area reference class j and class j in the map (Equation (4)). It is the probability that class j on the ground is mapped as the same class.

\hat{P}_{jj} the estimated proportion of area in cell jj of the error matrix (the error matrix of these estimated proportions Table 3).

Of the 220 pixels referred to as Forest, 205 were accurately categorized as Forest, 11 as Cultivated, and four as Bare land.

All 151 pixels referred to as Water was appropriately identified as such. 175 of the 189 pixels Urban were accurately classed as Urban; 6 were classified as Cultivated, and eight as Bare land.

Of the 65 pixels cited as Cultivated, 60 were accurately identified as Cultivated, three as Forest, and 2 as Bare ground.

Of the 124 pixels cited as Bare land, 111 were accurately classed as Bareland, 9 as Urban, and 4 as Cultivated.

$$\hat{P}_j = \frac{\hat{P}_{jj}}{\hat{P}_j} \times 100. \tag{4}$$

Overall Accuracy (OA)

The overall accuracy is the proportion of area classified correctly, and thus refers to the probability that a randomly selected j location on the map is classified correctly OA is calculated using Equation (5).

$$\hat{O} = \sum_{j=1}^n \tilde{y}_{jj} \times 100; \tag{5}$$

$$\hat{O} = 92.45\% \pm 1.88.$$

Table 4 shows the PA and user UA coefficients for different classifiers as a function of pixel sample size. The classification coefficient’s performance is impacted by the sample pixel size (UA: Bareland: 88.7% vs. Forest land: 93.18%) and the sample pixel size (UA: Bareland: 88.7% vs. Forest land: 93.18%), (PA: Cultivated land: 74.07% vs. Forest land: 98.55%). The RF model incorrectly classified 47 pixels, or 5.54% of the total, whereas 827 pixels were allocated correctly.

The non-representative pixel size of Cultivated land class Training samples has a detrimental impact on accuracy for both the producer and the consumer. In contrast, the higher class pixel sizes (Forest land and Urban land) give excellent quality accuracy for both UA and PA (Figures 4 and 5). Results show that the bigger pixel classes contain more pixels. It demonstrates that the bigger pixel classes benefit more from utilizing the pixel-based technique.

Table 4. Accuracy of RF classification for pixels sample size

Class	RF Classifier Parameters		No. of Pixels/Class		Accuracy		
	No. of Trees	Predictors	Training 80%	Testing 20%	Pixel misclassified	UA (%)	PA (%)
Forest	300	B3, B4, B5, B6, B7	209	25	15	93.18	98.55
Water	300	B3, B4, B5, B6, B7	145	36	0	100	100
Urban	300	B3, B4, B5, B6, B7	174	43	14	92.59	95.1
Cultivated	300	B3, B4, B5, B6, B7	63	16	5	92.3	74.07
Bareland	300	B3, B4, B5, B6, B7	111	28	13	88.7	88.8

Note: No. of Trees: Number of Trees; No. of Pixels/Class: Number of Pixel per class.

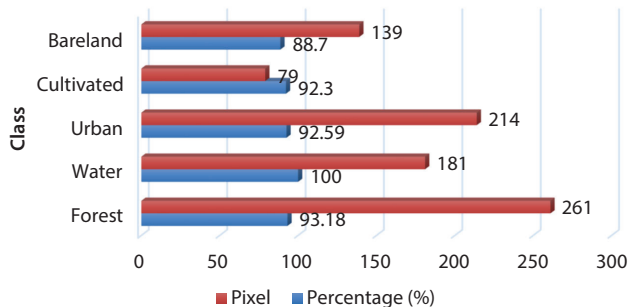


Figure 4. User Accuracy for each sample classifiers size

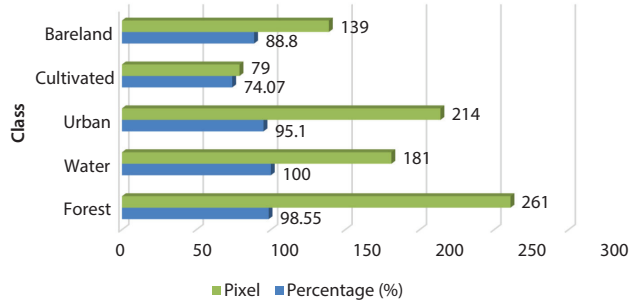


Figure 5. Producer accuracy for each sample classifiers size

Table 5. Land-use land-cover class area

Classes	Areas (km ²)
Forest	22 870.53
Water	951.97
Urban	555.06
Cultivated	12 284.66
Bareland	21 056.04

Table 5 shows that forest cover covers a significant part of the study area, accounting for 39.62%±1.2 of the total. Forest has a big representative area that is followed by bare land, which accounts for 36.48%±1.18; cultivated class, which accounts for 21.28%±0.90; water class, which accounts for 1.64%±0.25; and lastly, Urban class, which accounts for 0.96%±0.60. According to the results, forest and bare land cover the bulk of the study area, accounting for 39.62%±1.2 and 36.48%±1.18, respectively. Figure 6 depicts the LULC study area map.

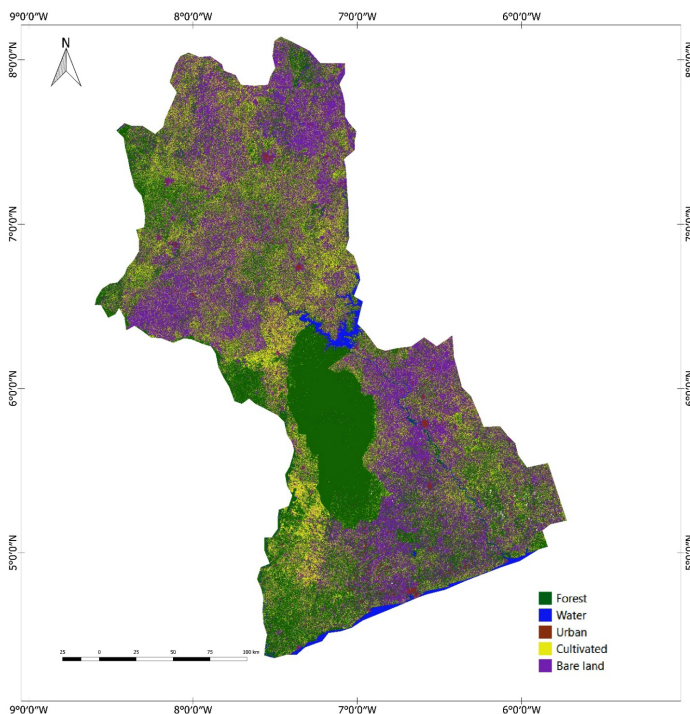


Figure 6. Map of study area land-cover/land-use classes 2020

3. Discussion

The classification results in this study were obtained at the pixel level with spatial resolutions of 30 m, the most significant degree of precision possible. The pixel-based RF classification technique yields acceptable results. This series of studies examines the efficacy of specific machine learning techniques, both aesthetically and statistically, against composite images. RF's observations showed a high accuracy rate of $94.02\% \pm 1.90$. VOA is considerably better than the VK coefficient of $92.25\% \pm 1.88$ of the images classified during the study period, and TOA is $99.85\% \pm 1.95$, and TK is $99.81\% \pm 1.95$, respectively. The high kappa value of the RF classification model is highly acceptable, and the model's accuracy performance is similar to a prior study that successfully distinguished LULC categories in diverse, realistic situations using RF (Rodriguez-Galiano et al., 2012b; Mellor et al., 2013).

The GEE land cover classification resulting from the analysis of Landsat 8 images provided very accurately provided very accurate findings. It is conceivable to conclude that the study's results are statistically acceptable. Aside from that, when the kappa value is more than 0.50, image analysis may provide excellent and relevant outcomes (Pontius, 2001) defined as formalized. As a result, the present classification with five classes is acceptable and enables the evaluation of land cover categorization throughout the study. Confusion errors may be seen in Forest, Urban, Cultivated, and Bare land categories. It's conceivable that the difficulty in visually differentiating these groups is due to the similarity of their spectral signatures. This is why the word Cultivated and Forest is often used interchangeably. This class may be found throughout the north, center, and south throughout the study area. This category may also include old plantations (coffee, cocoa, rubber, oil palm, and so on) and is often confused with it. This explains why there is miscommunication between the two groups in the first place (Forest and Cultivated).

Furthermore, due to the barren landscape, confusion errors between the classes (Urban and Bare land) were identified, which were also similar. The reported amounts of these perplexing errors, on the other hand, were minor. According to (Landis & Koch, 1977) and (de Certau et al., 1999), the findings obtained from the overall accuracy of the classifications are more significant than 95%, indicating that the results obtained from these classifications are excellent. The kappa coefficient is defined as the proportion of the classification result greater than or equal to 80%.

According to several research, a kappa coefficient in the range of 61 to 80% indicates a categorization result of "Good" or "Acceptable". Our VK is more than 90% means that our classification is reasonable. Because of the significant heterogeneity within LULC classes, RF in GEE identified soil classes based on their substantial heterogeneity, resulting in validation errors. The errors discovered in the LULC classes may be ascribed to the terrain's complexity and diversity, explained by (de Certau et al.,

1999). Classification errors will likely arise due to the challenges of selecting land-cover classes (Foody, 2002). After classification, the results show a significant percentage of cultivated land, indicating that this area is a central point of deforestation for developing and growing.

Table 4 shows the number of pixels in the error matrix correctly detected and misclassified by the RF classifier. Water features and trees, for example, perform very well, with accuracy rates above 95%. There was a mistake in categorizing land types such as cultivated land and forest land. For example (11 pixels not recognized as forest were classified as Cultivated land, and 4 pixels were allocated to the class Bareland). This misclassification reduced the producer's accuracy performance to 74.07% for Cultivated land and 88.8% for Bareland due to this inaccuracy. The classification errors in this experiment were most likely caused by the small number of collected training data. Indeed, several authors, such as Mellor et al. and Collin et al. (Mellor et al., 2015; Collins et al., 2020), have presented more significant evidence that the quality of the training samples causes these misclassifications gathered, overlapping classes, or the size of the study area (Foody et al., 2019).

Even though RF demonstrated superior classification performance in the other soil classes, a counter-performance was observed in classifying 14 pixels in the Urban land class, with 6 pixels assigned to the cultivated land class and 8 pixels assigned to the barren land class, respectively. Shetty et al. (Shetty, 2019) also made these results in his 2019 study in the Netherlands, where he uncovered categorization errors that resulted in low-performance producer accuracy coefficients.

Aside from the negative influence of the training site samples on the quality of the producer accuracy performance, another explanation for reducing the coefficients might be the low spatial resolution of the image data (30 m). This is because the study area is a tropical forest setting with a lot of cloud cover and darkness, making visibility challenging. The satellite data used in the study area, with a spatial resolution of 30 m, makes reliable differentiation between the various land use classes in the study area difficult without adding mistakes into the categorization.

Indeed, the classifiers vary the user accuracy and producer accuracy coefficients trend when the sample size changes. When we analyze the classification performances obtained, we see that the larger the sample size of the pixel/class, the better the RF performs in classification and provides excellent classification accuracies at the UA and PA levels of above 90%.

With a total of pixels in the five classes, we may consider the OA value of 92.45% obtained by RF during classification to be good, despite some classification errors. The OA and kappa coefficient values are roughly the same range as the multi-class image classification results obtained by Pal and Mather (2005) using the support vector machine classifier. A small sample set of 2700 pixels for seven crop types provided an accuracy of 87%.

Using the same RF method implemented in GEE, Wahap and Shafri (2020) obtained in his study, our results are slightly closer to theirs in terms of kappa accuracy (90.9%) and overall accuracy (94.8%). In comparison, theirs are somewhat closer in terms of OA (92.45%) and Kappa accuracy (90.9%). The matrix shows a precise categorization of the major forest kinds and a combination of cultivated and forest land.

Indeed, the minimal number of training samples collected at the Bareland and Cultivated land classes certainly hampered accuracy performance at the level of the producer accuracy coefficient values in this study. This conclusion is also likely attributable to the lower temporal and spectral resolution of the dataset utilized, which gave insufficient information to adequately separate the various agricultural types. Some authors recognized that to get improved performance in LULC classification; exceptionally high-quality training data are required (Song et al., 2016; Zhu et al., 2016; Shetty et al., 2021).

Conclusions

Remote sensing has shown to be pretty effective in different mapping types of LULC. In this study, Landsat 8OLI/TIRS data from 2020 were used to create a land-use map at the scale of the study area with a spatial resolution of 30 m. In this case, the GEE platform was used to develop the improved 2020 time-series dataset across the study area. The L8OLI/TIRS images were fed into a Pixel-based radiofrequency algorithm to finish building the LULC map of the study area. The obtained OA of 92.45%, TK of 99.81%, VK of 92.25%, OVA of 94.25%, and OTA of 99.85%, among other findings, show the remarkable ability of the proposed GEE technique to categorize the provided classes. Except for one class, the values of the PA and UA coefficients are much more than 90% in all but one of the other classes. Pure land makes up 88.88%, while cultivated land is 74.07%. The number of trees (300) and the five bands (B3, B4, B5, B6, B7) were significant predictors of the experiment's result. The small size of the training samples obtained and the minimal number of training samples collected affected the accuracy performance of the Cultivated land class. The classification method based on the Pixel Based approach could not provide a very high PA of the cultivated land class with the L8OLI/TIRS data because of the reduced spatial resolution. However, it would be fascinating to combine the pixel and object-based approaches with other auxiliary data, such as spectral obtained during different phenological seasons, to considerably improve the classification accuracy of the findings in a future study. The results of the categorization evaluation and map accuracy utilizing the pixel-based RF approach in GEE should assist policymakers in Côte d'Ivoire in appropriately managing and preserving biodiversity in the study area. In addition to monitoring forest areas and halting deforestation caused by agricultural operations.

Finally, the LULC map created as a result of this research will be useful in a variety of ways, notably in the development of a monitoring program for tracking long-term changes.

Funding

National Natural Science Fund Project for International and Regional Cooperation and Exchange "Sino-Argentinian Cooperation Research on Temperate Grassland Degradation: Current Status Assessment and Recovery Strategies" (32061123005) and National Natural Science Fund Project "Joint Species Distribution Model Based Grassland Degradation Assessment and Potential Risk Projection in Hulun Buir Steppe" (41971061).

Author contributions

Ideally, people who contributed to the work are listed in this section along with their contributions conceptualization (YX) and (ZK); methodology (CJAK); software (CJAK) and (CQ); validation (YX) and (ZK); formal analysis (CQ); investigation (DAK) (LSA); data curation (JKO) and (LSA); writing—original draft preparation (CJAK); writing—review, and editing (CJAK); visualization (DKA) and (JKO); supervision (YX) and (ZK); project administration (YX); funding acquisition (ZK). All authors have read and agreed to the published version of the manuscript.

References

- Adelabu, S., Mutanga, O., & Adam, E. (2015). Testing the reliability and stability of the internal accuracy assessment of random forest for classifying tree defoliation levels using different validation methods. *Geocarto International*, 30(7), 810–821. <https://doi.org/10.1080/10106049.2014.997303>
- Amani, M., Ghorbanian, A., Ahmadi, S. A., Kakooei, M., Moghimi, A., Mirmazloumi, S. M., Moghaddam, S. H. A., Mahdavi, S., Ghahremanloo, M., & Parsian, S. (2020). Google Earth Engine cloud computing platform for remote sensing big data applications: A comprehensive review. *IEEE Journal of Selected Topics in Applied Earth Observations and Remote Sensing*, 13, 5326–5350. <https://doi.org/10.1109/JSTARS.2020.3021052>
- Athey, S., Tibshirani, J., & Wager, S. (2019). Generalized random forests. *The Annals of Statistics*, 47, 1148–1178. <https://doi.org/10.1214/18-AOS1709>
- Azzari, G., & Lobell, D. (2017). Landsat-based classification in the cloud: An opportunity for a paradigm shift in land cover monitoring. *Remote Sensing of Environment*, 202, 64–74. <https://doi.org/10.1016/j.rse.2017.05.025>
- Barima, Y. S. S., Assalé, A. A. Y., Adiko, A. F. A. E., Kouakou, A. T. M., & Bamba, I. (2020). Dynamics of supply services provided by a protected forest in Côte d'Ivoire. *International Journal of Biodiversity and Conservation*, 12(4), 337–349. <https://doi.org/10.5897/IJBC2020.1436>
- Barima, Y. S. S., Kouakou, A. T. M., Bamba, I., Sangne, Y. C., Godron, M., Andrieu, J., & Bogaert, J. (2016). Cocoa crops are destroying the forest reserves of the classified forest of Haut-Sassandra (Ivory Coast). *Global Ecology and Conservation*, 8, 85–98. <https://doi.org/10.1016/j.gecco.2016.08.009>

- Bartlett, P., Freund, Y., Lee, W. S., & Schapire, R. E. (1998). Boosting the margin: A new explanation for the effectiveness of voting methods. *The Annals of Statistics*, 26(5), 1651–1686. <https://doi.org/10.1214/aos/1024691352>
- Belgiu, M., & Csillik, O. (2018). Sentinel-2 cropland mapping using pixel-based and object-based time-weighted dynamic time warping analysis. *Remote Sensing of Environment*, 204, 509–523. <https://doi.org/10.1016/j.rse.2017.10.005>
- Belgiu, M., & Drăguț, L. (2016). Random forest in remote sensing: A review of applications and future directions. *ISPRS Journal of Photogrammetry and Remote Sensing*, 114, 24–31. <https://doi.org/10.1016/j.isprsjprs.2016.01.011>
- Benz, S. A., Bayer, P., & Blum, P. (2017). Identifying anthropogenic anomalies in air, surface and groundwater temperatures in Germany. *Science of the Total Environment*, 584–585, 145–153. <https://doi.org/10.1016/j.scitotenv.2017.01.139>
- Bitty, E. A., Bi, S. G., Bene, J.-C. K., Kouassi, P. K., & McGraw, W. S. (2015). Cocoa farming and primate extirpation inside Cote d'Ivoire's protected areas. *Tropical Conservation Science*, 8, 95–113. <https://doi.org/10.1177/194008291500800110>
- Breiman, L. (2001). Random forests. *Machine Learning*, 45, 5–32. <https://doi.org/10.1023/A:1010933404324>
- Bwangoy, J.-R. B., Hansen, M. C., Roy, D. P., De Grandi, G., & Justice, C. O. (2010). Wetland mapping in the Congo Basin using optical and radar remotely sensed data and derived topographical indices. *Remote Sensing of Environment*, 114, 73–86. <https://doi.org/10.1016/j.rse.2009.08.004>
- Caruana, R., & Niculescu-Mizil, A. (2006). An empirical comparison of supervised learning algorithms. In *Proceedings of the 23rd International Conference on Machine Learning* (pp. 161–168). <https://doi.org/10.1145/1143844.1143865>
- Cecchi, P., Gourdin, F., Koné, S., Corbin, D., Etienne, J., & Casenave, A. (2009). Small reservoirs of Northern Côte d'Ivoire: Inventory and hydrological potentialities. *Science et changements planétaires/Sécheresse*, 20, 112–122. <https://doi.org/10.1684/sec.2009.0164>
- Chatelain, C., Dao, H., Gautier, L., & Spichiger, R. (2004). Forest cover changes in Côte d'Ivoire and Upper Guinea. In *Biodiversity of West African forests: Ecological atlas of woody plant species*, (pp. 15–32). CABI Publishing. <https://doi.org/10.1079/9780851997346.0015>
- Chatelain-Ponroy, S. (2010). Une voie de compréhension du contrôle de gestion dans les organisations non marchandes: la métaphore de l'iceberg. *Politiques et management public*, 27, 73–103. <https://doi.org/10.4000/pmp.3005>
- Cihlar, J. (2000). Land cover mapping of large areas from satellites: Status and research priorities. *International Journal of Remote Sensing*, 21, 1093–1114. <https://doi.org/10.1080/014311600210092>
- Cohen, W. B., Yang, Z., & Kennedy, R. (2010). Detecting trends in forest disturbance and recovery using yearly Landsat time series: 2. TimeSync – Tools for calibration and validation. *Remote Sensing of Environment*, 114(12), 2911–2924. <https://doi.org/10.1016/j.rse.2010.07.010>
- Collins, L., McCarthy, G., Mellor, A., Newell, G., & Smith, L. (2020). Training data requirements for fire severity mapping using Landsat imagery and random forest. *Remote Sensing of Environment*, 245, 111839. <https://doi.org/10.1016/j.rse.2020.111839>
- Congalton, R. G., & Green, K. (2019). *Assessing the accuracy of remotely sensed data: Principles and practices*. CRC Press. <https://doi.org/10.1201/9780429052729>
- Corona, P., Cartisano, R., Salvati, R., Chirici, G., Floris, A., Di Martino, P., Marchetti, M., Scrinzi, G., Clementel, F., & Travalini, D. (2012). Airborne Laser Scanning to support forest resource management under alpine, temperate and Mediterranean environments in Italy. *European Journal of Remote Sensing*, 45(1), 27–37. <https://doi.org/10.5721/EuJRS20124503>
- e Certau, M., Giard, L., & Mayol, P. (1999). *La invención de lo cotidiano 2: Habitar, cocinar* (pp. 151–174). El Oficio de la Historia.
- Desanker, P., Frost, P., Justice, C., & Scholes, R. (1997). *The Miombo Network: Framework for a terrestrial transect study of land-use and land-cover change in the miombo ecosystems of Central Africa* (IGBP Global change report). IGBP. <https://digital.library.unt.edu/ark:/67531/metadc11998/>
- Foga, S., Scaramuzza, P. L., Guo, S., Zhu, Z., Dilley Jr, R. D., Beckmann, T., Schmidt, G. L., Dwyer, J. L., Hughes, M. J., & Laue, B. (2017). Cloud detection algorithm comparison and validation for operational Landsat data products. *Remote Sensing of Environment*, 194, 379–390. <https://doi.org/10.1016/j.rse.2017.03.026>
- Fonseka, H., Zhang, H., Sun, Y., Su, H., Lin, H., & Lin, Y. (2019). Urbanization and its impacts on land surface temperature in Colombo metropolitan area, Sri Lanka, from 1988 to 2016. *Remote Sensing*, 11, 957. <https://doi.org/10.3390/rs11080957>
- Foody, G. M. (2002). Status of land cover classification accuracy assessment. *Remote Sensing of Environment*, 80(1), 185–201. [https://doi.org/10.1016/S0034-4257\(01\)00295-4](https://doi.org/10.1016/S0034-4257(01)00295-4)
- Foody, G. M., Ling, F., Boyd, D. S., Li, X., & Wardlaw, J. (2019). Earth observation and machine learning to meet sustainable development goal 8.7: Mapping sites associated with slavery from space. *Remote Sensing*, 11, 266. <https://doi.org/10.3390/rs11030266>
- Forghani-Zadeh, H. P., & Rincón-Mora, G. A. (2007). An accurate, continuous, and lossless self-learning CMOS current-sensing scheme for inductor-based DC-DC converters. *IEEE Journal of Solid-State Circuits*, 42(3), 665–679. <https://doi.org/10.1109/JSSC.2006.891721>
- Ge, Y., Hu, S., Ren, Z., Jia, Y., Wang, J., Liu, M., Zhang, D., Zhao, W., Luo, Y., & Fu, Y. (2019). Mapping annual land use changes in China's poverty-stricken areas from 2013 to 2018. *Remote Sensing of Environment*, 232, 111285. <https://doi.org/10.1016/j.rse.2019.111285>
- Ghorbanian, A., Kakooei, M., Amani, M., Mahdavi, S., Mohammadzadeh, A., & Hasanlou, M. (2020). Improved land cover map of Iran using Sentinel imagery within Google Earth Engine and a novel automatic workflow for land cover classification using migrated training samples. *ISPRS Journal of Photogrammetry and Remote Sensing*, 167, 276–288. <https://doi.org/10.1016/j.isprsjprs.2020.07.013>
- Gislason, P. O., Benediktsson, J. A., & Sveinsson, J. R. (2006). Random forests for land cover classification. *Pattern Recognition Letters*, 27(4), 294–300. <https://doi.org/10.1016/j.patrec.2005.08.011>
- Gorelick, N., Hancher, M., Dixon, M., Ilyushchenko, S., Thau, D., & Moore, R. (2017). Google Earth Engine: Planetary-scale geospatial analysis for everyone. *Remote Sensing of Environment*, 202, 18–27. <https://doi.org/10.1016/j.rse.2017.06.031>
- Griffiths, P., van der Linden, S., Kuemmerle, T., Hostert, P. (2013). A pixel-based Landsat compositing algorithm for large area land cover mapping. *IEEE Journal of Selected Topics in Applied Earth Observations and Remote Sensing*, 6(5), 2088–2101. <https://doi.org/10.1109/JSTARS.2012.2228167>
- Gudmann, A., Csikós, N., Szilassi, P., & Mucsi, L. (2020). Improvement in satellite image-based land cover classification with landscape metrics. *Remote Sensing*, 12, 3580. <https://doi.org/10.3390/rs12213580>

- Hansen, M. C., Potapov, P. V., Moore, R., Hancher, M., Turubanova, S. A., Tyukavina, A., Thau, D., Stehman, S. V., Goetz, S. J., & Loveland, T. R. (2013). High-resolution global maps of 21st-century forest cover change. *Science*, 342(6160), 850–853. <https://doi.org/10.1126/science.1244693>
- Hansen, M. C., Roy, D. P.; Lindquist, E., Adusei, B., Justice, C. O., & Altstatt, A. (2008). A method for integrating MODIS and Landsat data for systematic monitoring of forest cover and change in the Congo Basin. *Remote Sensing of Environment*, 112(5), 2495–2513. <https://doi.org/10.1016/j.rse.2007.11.012>
- Hatwell, J., Gaber, M. M., & Azad, R. M. A. (2020). CHIRPS: Explaining random forest classification. *Artificial Intelligence Review*, 53, 5747–5788. <https://doi.org/10.1007/s10462-020-09833-6>
- Irons, J. R., Dwyer, J. L., & Barsi, J. A. (2012). The next Landsat satellite: The Landsat data continuity mission. *Remote Sensing of Environment*, 122, 11–21. <https://doi.org/10.1016/j.rse.2011.08.026>
- Joshi, A. R., Dinerstein, E., Wikramanayake, E., Anderson, M. L., Olson, D., Jones, B. S., Seidensticker, J., Lumpkin, S., Hansen, M. C., Sizer, N. C., Davis, C. L., Palminteri, S., & Hahn, N. R. (2016). Tracking changes and preventing loss in critical tiger habitat. *Science Advances*, 2(4), 1–8. <https://doi.org/10.1126/sciadv.1501675>
- Kennedy, R. E., Yang, Z., & Cohen, W. B. (2010). Detecting trends in forest disturbance and recovery using yearly Landsat time series: 1. LandTrendr – Temporal segmentation algorithms. *Remote Sensing of Environment*, 114(12), 2897–2910. <https://doi.org/10.1016/j.rse.2010.07.008>
- Keyport, R. N., Oommen, T., Martha, T. R., Sajinkumar, K., & Gierke, J. S. (2018). A comparative analysis of pixel-and object-based detection of landslides from very high-resolution images. *International Journal of Applied Earth Observation and Geoinformation*, 64, 1–11. <https://doi.org/10.1016/j.jag.2017.08.015>
- Koua, K. A. N., Kpangui, K. B., & Barima, Y. S. S. (2020). Impact of cocoa cultivation in the forest-savannah transition zone of western Côte d'Ivoire. *International Journal of Biodiversity and Conservation*, 12(4), 291–304. <https://doi.org/10.5897/IJBC2020.1430>
- Kouassi, J., Gyau, A., Diby, L., Bene, Y., & Kouamé, C. (2021). Assessing land use and land cover change and farmers' perceptions of deforestation and land degradation in South-West Côte d'Ivoire, West Africa. *Land*, 10, 429. <https://doi.org/10.3390/land10040429>
- Landis, J. R., & Koch, G. G. (1977). An application of hierarchical kappa-type statistics in the assessment of majority agreement among multiple observers. *Biometrics*, 33(2), 363–374. <https://doi.org/10.2307/2529786>
- Liu, X., Hu, G., Chen, Y., Li, X., Xu, X., Li, S., Pei, F., & Wang, S. (2018). High-resolution multi-temporal mapping of global urban land using Landsat images based on the Google Earth Engine Platform. *Remote Sensing of Environment*, 209, 227–239. <https://doi.org/10.1016/j.rse.2018.02.055>
- Lu, D., Weng, Q., & Li, G. (2006). Residential population estimation using a remote sensing derived impervious surface approach. *International Journal of Remote Sensing*, 27(16), 3553–3570. <https://doi.org/10.1080/01431160600617202>
- Luo, J., Ma, X., Chu, Q., Xie, M., & Cao, Y. (2021). Characterizing the up-to-date land-use and land-cover change in Xiong'an New Area from 2017 to 2020 using the multi-temporal Sentinel-2 images on Google Earth Engine. *ISPRS International Journal of Geo-Information*, 10(7), 464. <https://doi.org/10.3390/ijgi10070464>
- Magidi, J., Nhamo, L., Mpandeli, S., & Mabhaudhi, T. (2021). Application of the Random Forest classifier to map irrigated areas using Google Earth Engine. *Remote Sensing*, 13(5), 876. <https://doi.org/10.3390/rs13050876>
- Mahdianpari, M., Salehi, B., Mohammadimanesh, F., Homayouni, S., & Gill, E. (2019). The first wetland inventory map of Newfoundland at a spatial resolution of 10 m using Sentinel-1 and Sentinel-2 data on the Google Earth Engine cloud computing platform. *Remote Sensing*, 11(1), 43. <https://doi.org/10.3390/rs11010043>
- Mas, J. (2000). Une revue des méthodes et des techniques de télédétection du changement. *Canadian Journal of Remote Sensing*, 26(4), 349–362. <https://doi.org/10.1080/07038992.2000.10874785>
- Meher, P. K., Sahu, T. K., & Rao, A. R. (2016). Prediction of donor splice sites using random forest with a new sequence encoding approach. *BioData Mining*, 9, 1–25. <https://doi.org/10.1186/s13040-016-0086-4>
- Mellor, A., & Boukir, S. (2017). Exploring diversity in ensemble classification: Applications in large area land cover mapping. *ISPRS Journal of Photogrammetry and Remote Sensing*, 129, 151–161. <https://doi.org/10.1016/j.isprsjprs.2017.04.017>
- Mellor, A., Boukir, S., Haywood, A., & Jones, S. (2015). Exploring issues of training data imbalance and mislabelling on random forest performance for large area land cover classification using the ensemble margin. *ISPRS Journal of Photogrammetry and Remote Sensing*, 105, 155–168. <https://doi.org/10.1016/j.isprsjprs.2015.03.014>
- Mellor, A., Haywood, A., Stone, C., & Jones, S. (2013). The performance of random forests in an operational setting for large area sclerophyll forest classification. *Remote Sensing*, 5, 2838–2856. <https://doi.org/10.3390/rs5062838>
- Moore, R., & Hansen, M. (2011). Google Earth Engine: A new cloud-computing platform for global-scale earth observation data and analysis. In *Proceedings of the AGU Fall Meeting* (Abstract id. IN43C-02). <https://ui.adsabs.harvard.edu/abs/2011AGUFMIN43C..02M/abstract>
- Mountrakis, G., Im, J., & Ogole, C. (2011). Support vector machines in remote sensing: A review. *ISPRS Journal of Photogrammetry and Remote Sensing*, 66, 247–259. <https://doi.org/10.1016/j.isprsjprs.2010.11.001>
- Naboureh, A., Ebrahimy, H., Azadbakht, M., Bian, J., & Amani, M. (2020). RUESVMs: An ensemble method to handle the class imbalance problem in land cover mapping using Google Earth Engine. *Remote Sensing*, 12(21), 3484. <https://doi.org/10.3390/rs12213484>
- Nery, T., Sadler, R., Solis-Aulestia, M., White, B., Polyakov, M., & Chalak, M. (2016). Comparing supervised algorithms in Land Use and Land Cover classification of a Landsat time-series. In *Proceedings of the 2016 IEEE International Geoscience and Remote Sensing Symposium (IGARSS)* (pp. 5165–5168), Beijing, China. <https://doi.org/10.1109/IGARSS.2016.7730346>
- Nyland, K. E., Gunn, G. E., Shiklomanov, N. I., Engstrom, R. N., & Streletskiy, D. A. (2018). Land cover change in the lower Yenisei River using dense stacking of landsat imagery in Google Earth Engine. *Remote Sensing*, 10(8), 1226. <https://doi.org/10.3390/rs10081226>
- Olofsson, P., Foody, G. M., Herold, M., Stehman, S. V., Woodcock, C. E., & Wulder, M. A. (2014). Good practices for estimating area and assessing accuracy of land change. *Remote Sensing of Environment*, 148, 42–57. <https://doi.org/10.1016/j.rse.2014.02.015>
- Pal, M., & Mather, P. (2005). Support vector machines for classification in remote sensing. *International Journal of Remote*

- Sensing*, 26(5), 1007–1011. <https://doi.org/10.1080/01431160512331314083>
- Pareeth, S., Karimi, P., Shafiei, M., & De Fraiture, C. (2019). Mapping agricultural landuse patterns from time series of Landsat 8 using random forest based hierarchical approach. *Remote Sensing*, 11(5), 601. <https://doi.org/10.3390/rs11050601>
- Parente, L., & Ferreira, L. (2018). Assessing the spatial and occupation dynamics of the Brazilian pastures based on the automated classification of MODIS images from 2000 to 2016. *Remote Sensing*, 10, 606. <https://doi.org/10.3390/rs10040606>
- Phan, T. N., Kuch, V., & Lehnert, L. W. (2020). Land cover classification using Google Earth Engine and Random Forest classifier – The role of image composition. *Remote Sensing*, 12(15), 2411. <https://doi.org/10.3390/rs12152411>
- Plourde, L., & Congalton, R. G. (2003). Sampling method and sample placement. *Photogrammetric Engineering & Remote Sensing*, 69(3), 289–297. <https://doi.org/10.14358/PERS.69.3.289>
- Pontius, R. (2001). Quantification error versus location error in comparison of categorical maps. *Photogrammetric Engineering & Remote Sensing*, 66, 1011–1016.
- Probst, P., & Boulesteix, A.-L. (2017). To tune or not to tune the number of trees in random forest. *Journal of Machine Learning Research*, 18, 6673–6690.
- Qu, L., Li, M., Chen, Z., & Zhi, J. (2021). A modified self-adaptive method for mapping annual 30-m land use/land cover using Google Earth Engine: A case study of Yangtze River Delta. *Chinese Geographical Science*, 31, 782–794. <https://doi.org/10.1007/s11769-021-1226-4>
- Ravanelli, R., Nascetti, A., Cirigliano, R. V., Di Rico, C., Leuzzi, G., Monti, P., & Crespi, M. (2018). Monitoring the impact of land cover change on surface urban heat island through Google Earth Engine: Proposal of a global methodology, first applications and problems. *Remote Sensing*, 10(9), 1488. <https://doi.org/10.3390/rs10091488>
- Robinson, N. P., Allred, B. W., Jones, M. O., Moreno, A., Kimball, J. S., Naugle, D. E., Erickson, T. A., & Richardson, A. D. (2017). A dynamic Landsat derived normalized difference vegetation index (NDVI) product for the conterminous United States. *Remote Sensing*, 9(8), 863. <https://doi.org/10.3390/rs9080863>
- Rodriguez-Galiano, V. F., Ghimire, B., Rogan, J., Chica-Olmo, M., & Rigol-Sanchez, J. P. (2012b). An assessment of the effectiveness of a random forest classifier for land-cover classification. *ISPRS Journal of Photogrammetry and Remote Sensing*, 67, 93–104. <https://doi.org/10.1016/j.isprsjprs.2011.11.002>
- Rodriguez-Galiano, V., Chica-Olmo, M., Abarca-Hernandez, F., Atkinson, P. M., & Jeganathan, C. (2012a). Random Forest classification of Mediterranean land cover using multi-seasonal imagery and multi-seasonal texture. *Remote Sensing of Environment*, 121, 93–107. <https://doi.org/10.1016/j.rse.2011.12.003>
- Ruf, F., & Zadi, H. (1998). *Cocoa: From deforestation to reforestation*. https://agritrop.cirad.fr/390123/1/document_390123.pdf
- Ruf, F., Schroth, G., & Doffangui, K. (2015). Climate change, cocoa migrations and deforestation in West Africa: What does the past tell us about the future? *Sustainability Science*, 10, 101–111. <https://doi.org/10.1007/s11625-014-0282-4>
- Schmidt, J., Marques, M. R., Botti, S., & Marques, M. A. (2019). Recent advances and applications of machine learning in solid-state materials science. *npj Computational Materials*, 5, 1–36. <https://doi.org/10.1038/s41524-019-0221-0>
- Shetty, S. (2019). *Analysis of machine learning classifiers for LULC classification on Google Earth Engine*. University of Twente.
- Shetty, S., Gupta, P. K., Belgiu, M., & Srivastav, S. (2021). Assessing the effect of training sampling design on the performance of machine learning classifiers for land cover mapping using multi-temporal remote sensing data and Google Earth Engine. *Remote Sensing*, 13(8), 1433. <https://doi.org/10.3390/rs13081433>
- Song, X.-D., Brus, D. J., Liu, F., Li, D.-C., Zhao, Y.-G., Yang, J.-L., & Zhang, G.-L. (2016). Mapping soil organic carbon content by geographically weighted regression: A case study in the Heihe River Basin, Chin. *Geoderma*, 261, 11–22. <https://doi.org/10.1016/j.geoderma.2015.06.024>
- Stehman, S. V. (2009). Sampling designs for accuracy assessment of land cover. *International Journal of Remote Sensing*, 30, 5243–5272. <https://doi.org/10.1080/01431160903131000>
- Story, M., & Congalton, R. G. (1986). Accuracy assessment: A user's perspective. *Photogrammetric Engineering & Remote Sensing*, 52(3), 397–399.
- Strahler, A. H., Boschetti, L., Foody, G. M., Friedl, M. A., Hansen, M. C., Herold, M., Mayaux, P., Morissette, J. T., Stehman, S. V., & Woodcock, C. E. (2006). *Global land cover validation: Recommendations for evaluation and accuracy assessment of global land cover maps* (EUR 22156 EN). European Communities.
- Tassi, A., Gigante, D., Modica, G., Di Martino, L., & Vizzari, M. (2021). Pixel-vs. object-based Landsat 8 data classification in Google Earth engine using random forest: The case study of Maiella National Park. *Remote Sensing*, 13(12), 2299. <https://doi.org/10.3390/rs13122299>
- Tatsumi, K., Yamashiki, Y., Torres, M. A. C., & Taïpe, C. L. R. (2015). Crop classification of upland fields using Random forest of time-series Landsat 7 ETM+ data. *Computers and Electronics in Agriculture*, 115, 171–179. <https://doi.org/10.1016/j.compag.2015.05.001>
- Thébault, E., & Loreau, M. (2005). Trophic interactions and the relationship between species diversity and ecosystem stability. *The American Naturalist*, 166, E95–E114. <https://doi.org/10.1086/444403>
- Toosi, N. B., Soffianian, A. R., Fakheran, S., Pourmanafi, S., Ginzler, C., & Waser, L. T. (2019). Comparing different classification algorithms for monitoring mangrove cover changes in southern Iran. *Global Ecology and Conservation*, 19, e00662. <https://doi.org/10.1016/j.gecco.2019.e00662>
- Traganos, D., Aggarwal, B., Poursanidis, D., Topouzelis, K., Chrysoulakis, N., & Reinartz, P. (2018). Towards global-scale seagrass mapping and monitoring using Sentinel-2 on Google Earth Engine: The case study of the aegean and ionian seas. *Remote Sensing*, 10(8), 1227. <https://doi.org/10.3390/rs10081227>
- Verburg, P. H., Kok, K., Pontius, R. G. Jr., & Veldkamp, A. (2006). Modeling land-use and land-cover change. In E. F. Lambin & H. Geist (Eds.), *Land-use and land-cover change: Local processes and global impacts* (pp. 117–135). Springer. https://doi.org/10.1007/3-540-32202-7_5
- Wahap, N., & Shafri, H. Z. (2020). Utilization of Google Earth Engine (GEE) for land cover monitoring over Klang Valley, Malaysia. In *Proceedings of the IOP Conference Series: Earth and Environmental Science* (Vol. 540, p. 012003). IOP Publishing. <https://doi.org/10.1088/1755-1315/540/1/012003>
- Walker, R. (2004). Theorizing land-cover and land-use change: the case of tropical deforestation. *International Regional Science Review*, 27(3), 247–270. <https://doi.org/10.1177/0160017604266026>
- Wang, Z., Lai, C., Chen, X., Yang, B., Zhao, S., & Bai, X. (2015). Flood hazard risk assessment model based on random forest.

- Journal of Hydrology*, 527, 1130–1141.
<https://doi.org/10.1016/j.jhydrol.2015.06.008>
- White, F. (1983). *The vegetation of Africa: A descriptive memoir to accompany the UNESCO/AETFAT/UNSO vegetation map of Africa*. Unesco.
- Xiong, J., Thenkabail, P. S., Tilton, J. C., Gumma, M. K., Teluguntla, P., Oliphant, A., Congalton, R. G., Yadav, K., & Gorelick, N. (2017). Nominal 30-m cropland extent map of continental Africa by integrating pixel-based and object-based algorithms using Sentinel-2 and Landsat-8 data on Google Earth Engine. *Remote Sensing*, 9(10), 1065.
<https://doi.org/10.3390/rs9101065>
- Zeferino, L. B., de Souza, L. F. T., do Amaral, C. H., Fernandes Filho, E. I., & de Oliveira, T. S. (2020). Does environmental data increase the accuracy of land use and land cover classification? *International Journal of Applied Earth Observation and Geoinformation*, 91, 102128.
<https://doi.org/10.1016/j.jag.2020.102128>
- Zhu, Z., Gallant, A. L., Woodcock, C. E., Pengra, B., Olofsson, P., Loveland, T. R., Jin, S., Dahal, D., Yang, L., & Auch, R. F. (2016). Optimizing selection of training and auxiliary data for operational land cover classification for the LCMAP initiative. *ISPRS Journal of Photogrammetry and Remote Sensing*, 122, 206–221. <https://doi.org/10.1016/j.isprsjprs.2016.11.004>